

# Life-Threatening Arrhythmia Verification in ICU Patients Using the Joint Cardiovascular Dynamical Model and a Bayesian Filter

Omid Sayadi\*, *Student Member, IEEE*, and Mohammad B. Shamsollahi, *Member, IEEE*

**Abstract**—In this paper, a novel nonlinear joint dynamical model is presented, which is based on a set of coupled ordinary differential equations of motion and a Gaussian mixture model representation of pulsatile cardiovascular (CV) signals. In the proposed framework, the joint interdependences of CV signals are incorporated by assuming a unique angular frequency that controls the limit cycle of the heart rate. Moreover, the time consequence of CV signals is controlled by the same phase parameter that results in the space dimensionality reduction. These joint equations together with linear assignments to observation are further used in the Kalman filter structure for estimation and tracking. Moreover, we propose a measure of signal fidelity by monitoring the covariance matrix of the innovation signals throughout the filtering procedure. Five categories of life-threatening arrhythmias were verified by simultaneously tracking the signal fidelity and the polar representation of the CV signal estimations. We analyzed data from Physiobank multiparameter databases (MIMIC I and II). Performance evaluation results demonstrated that the sensitivity of the detection ranges over 93.50% and 100.00%. In particular, the addition of more CV signals improved the positive predictivity of the proposed method to 99.27% for the total arrhythmic types. The method was also used for false arrhythmia suppression issued by ICU monitors, with an overall false suppression rate reduced from 42.3% to 9.9%. In addition, false critical ECG arrhythmia alarm rates were found to be, on average, 42.3%, with individual rates varying between 16.7% and 86.5%. The results illustrate that the method can contribute to, and enhance the performance of clinical life-threatening arrhythmia detection.

**Index Terms**—Arrhythmia verification, cardiovascular (CV) signals, extended Kalman filter (EKF), false alarm (FA) suppression, joint dynamical model, signal fidelity.

## I. INTRODUCTION

CURRENTLY, electrocardiogram (ECG) analysis is routinely used as the first tool for initial screening of cardiovascular (CV) diseases and noninvasive diagnosis of life-threatening arrhythmias in clinical practice. Analysis of the ECG, as a noninvasive and low-cost method, provides valuable clinical information and, therefore, remains the benchmark

method for cardiac arrhythmia detection [1]. However, commercial monitoring systems, and especially the ICU monitors, often include the capability to monitor other CV signals, heart rate, and several statistics of pressure signals [2]. Such information can come from signals that are related to cardiac function but are either different in nature or measured in a location remote to the heart and are, therefore, unlikely to exhibit the same types of noise and artifacts as the ECG. Signals with pulsatile waveforms offer the additional benefit of having features indicative of the cardiac cycle, which can be later compared to timing and morphology of the ECG features.

The pivotal role of neural mechanisms in CV pathophysiology has been postulated in the past few decades. It is known that CV signals contain parameters of clinical significance and hold beat-to-beat variability that reflects the interaction between the disturbances on CV variables and the regulating systems response [3]. The observation that CV variables exhibit, beat-to-beat, small nonrandom changes around their mean values with a frequency well below the heart rate has been interpreted as evidence of the CV regulation [4]. Regulation of CV variables is now assumed to be the result of the action of multiple feedback systems (e.g., chemoreceptive and baroreceptive) and self-sustained autonomous oscillators situated not only at brain stem level (e.g., respiratory and vasomotor centers) but also at spinal and at peripheral level (e.g., vasomotor districts) [5], [6]. Studies have shown that different physiological conditions and pathological disorders result in the fluctuations of the CV signals [7]. It is currently accepted that the joint study of ECG, and specifically the heart rate variability, and arterial blood pressure (ABP) allows accessing the baroreceptor reflex sensitivity as a measure of the integrity of the autonomic nervous system [8]. For this reason, the interpretation of CV regulation mechanisms should be assessed within the framework of the dynamics of the sympatho-vagal interactions that govern the instantaneous performance of the CV system [9], [10]. Thus, the regulatory mechanisms that underlie CV beat-to-beat variability should be approached in a joint dynamic manner.

The modern ICU employs an impressive array of technologies that results in the generation of a rich set of clinical data used to guide patient care. The enormous amount of ICU data and its poor organization make its integration and interpretation time consuming and inefficient. The resultant data overload may actually hinder the diagnostic process, and may even lead to neglect of relevant data, resulting in errors and complications in ICU care. In the long term, automated clinical decision support

Manuscript received July 20, 2010; revised September 25, 2010; accepted October 19, 2010. Date of publication February 14, 2011; date of current version September 21, 2011. Asterisk indicates corresponding author.

\*O. Sayadi is with the Biomedical Signal and Image Processing Laboratory (BiSIPL), School of Electrical Engineering, Sharif University of Technology, Tehran 11365-9363, Iran (e-mail: osayadi@ee.sharif.edu).

M. B. Shamsollahi is with the Biomedical Signal and Image Processing Laboratory (BiSIPL), School of Electrical Engineering, Sharif University of Technology, Tehran 11365-9363, Iran (e-mail: mbshams@sharif.edu).

Digital Object Identifier 10.1109/TBME.2010.2093898

systems are needed to explain the rich and complex volume of data from clinical observations and bedside monitors.

Despite the success of statistic and dynamic modeling approaches toward ECG analysis, they have not been widely applied to solve estimation and tracking problems involving other CV signals which is due, in part, to the unavailability of statistical or dynamical models for these signals. In a pioneer work, McNames and Aboy proposed a statistical model of CV signals that was based on an autoregressive formulation for the state variables [11]. The model incorporated some parameters of clinical interest relevant to ABP, pulse oximetry, and intracranial pressure that were related to the state variables using a sum of sinusoidal functions. This model suffered from the lack of morphology information as well as the joint synchronous dynamic relations of the CV signals.

In this paper, we develop a joint dynamical state-space model that is designed for being used in Bayesian estimation procedures such as the Kalman filter (KF) to provide synchronized estimations of CV signals, including the ECG, ABP, photoplethysmograph (PPG), central venous pressure (CVP), and pulmonary artery pressure (PAP). The proposed novel framework incorporates a set of multiple CV signals in a unique model, for simultaneous estimation and tracking purposes. We illustrate its ability to solve relevant problems in life-threatening arrhythmia verification in ICU patients, including the detection and status determination of cardiac anomalies. The verification procedure is then employed for false alarm suppression. As an advantage, the Bayesian estimator is adapted to the temporal characteristics of the observed signals. Hence, unlike popular detection algorithms [12]–[15] and suppression systems [16], [17], the proposed technique is not based upon thresholding, which improves the detection accuracy of the method.

This paper is organized as follows. In Section II, the joint dynamical state-space model is presented. Section III provides relevant background on the theory of the Kalman estimation. In Section IV, our proposed algorithm for life-threatening arrhythmia verification is explained in detail. Section V is devoted to simulation results. Finally, discussion and conclusion are provided in Section VI.

## II. JOINT DYNAMICAL STATE-SPACE MODEL

Following [18], [19], and using an explicit phase variable as an indicator of the angular locations of the P, Q, R, S, and T waves [20], [21], the dynamics of the cardiac signal and its relation to the discrete measurements can be modeled in the form of a state space. The process and observation equations of this formulation are given by

*Process equation:*

$$\begin{cases} \varphi_{k+1} = (\varphi_k + \omega_k \delta) \bmod(2\pi) \\ s_{k+1} = s_k - \omega_k \delta \text{ GMM}(\alpha_i, b_i, \theta_i, k) + \eta_k \end{cases} \quad (1)$$

*Observation equation:*

$$\begin{cases} \phi_k = \varphi_k + u_{1k} \\ z_k = s_k + u_{2k} \end{cases} \quad (2)$$

where the cardiac phase  $\varphi \in [-\pi, \pi]$  and the ECG signal  $s$  are the state variables,  $\delta$  is the sampling period,  $\omega = 2\pi f$ ,

is the beat-to-beat heart rate, and  $\eta$  is the baseline perturbation term. In (2), the phase observation  $\phi$  is a synthetic signal formed by linear assignment of a phase between  $-\pi$  and  $\pi$  [21]. The second observation  $z$  represents the noisy ECG measurement, and  $u_1$  and  $u_2$  are the observation noises. The Gaussian mixture model (GMM) representation for the ECG is defined as:

$$\text{GMM}(\alpha_i, b_i, \Delta\theta_i, k) = \sum_{i \in \{P, Q, R, S, T\}} \frac{\alpha_{i_k}}{b_{i_k}^2} \Delta\theta_i \exp\left(-\frac{\Delta\theta_{i_k}^2}{2b_{i_k}^2}\right) \quad (3)$$

where  $\Delta\theta_{i_k} = (\varphi_k - \theta_{i_k}) \bmod(2\pi)$ . The first equation in (1) generates a circular trajectory rotating with the frequency of the heart rate. The ECG signal is modeled by a summation of Gaussian functions with amplitudes  $\alpha_i$ , widths  $b_i$ , and located at rotational angles  $\theta_i$ . In the process equation (1),  $\omega$ ,  $\eta$ , and the Gaussian kernel parameters  $\alpha_i$ ,  $b_i$ ,  $\theta_i$  are assumed as independent identically distributed Gaussian random variables considered as process noises.

In order to develop a joint formulation, we must first express the relationship between the variables of interest and the observed signals in the form of

$$\begin{cases} \underline{x}_{k+1} = f(\underline{x}_k, \underline{w}_k, k) \\ \underline{y}_k = g(\underline{x}_k, \underline{v}_k, k) \end{cases} \quad (4)$$

and afterward, it is necessary to find efficient relations—that have physiological correspondences—between the parameters of the model. In (4),  $\underline{x}_k$  is a vector that represents the states of the system,  $\underline{w}_k$  is the process noise vector with a covariance matrix  $Q$ ,  $\underline{y}_k$  is a vector of the observed signals, and  $\underline{v}_k$  is the observation or measurement noise vector with a covariance matrix  $R$ . The state evolution function  $f$  and the observation relation  $g$  collectively comprise the statistical state-space model of the process. The most critical decision in adopting the KF framework is to design these two models in a manner that incorporates known physiologic mechanisms and uses a compact state vector that contains the variables of interest.

To develop a joint dynamical model for a set of  $N$  CV signals with morphological considerations, it is possible to use a combination of the model proposed by McSharry *et al.* [18]. In fact, we can use the same set of evolution functions with different parameters for each individual signal, to which [similar to (1)], two state variables are assigned, which results in a diagonal model given by

*Process equation:*

$$\begin{cases} \varphi_{k+1}^1 = F_0(\varphi_k^1, \omega_k^1, k) \\ s_{k+1}^1 = F_1(s_k^1, \varphi_k^1, \omega_k^1, \alpha_i^1, b_i^1, \theta_i^1, \eta_k^1, k) \\ \varphi_{k+1}^2 = F_0(\varphi_k^2, \omega_k^2, k) \\ s_{k+1}^2 = F_1(s_k^2, \varphi_k^2, \omega_k^2, \alpha_i^2, b_i^2, \theta_i^2, \eta_k^2, k) \\ \vdots \\ \varphi_{k+1}^N = F_0(\varphi_k^N, \omega_k^N, k) \\ s_{k+1}^N = F_1(s_k^N, \varphi_k^N, \omega_k^N, \alpha_i^N, b_i^N, \theta_i^N, \eta_k^N, k) \end{cases} \quad (5)$$

Observation equation:

$$\begin{cases} \phi_k^1 = \varphi_k^1 + u_{1_k}^1 \\ z_k^1 = s_k^1 + u_{2_k}^1 \\ \vdots \\ \phi_k^N = \varphi_k^N + u_{1_k}^N \\ z_k^N = s_k^N + u_{2_k}^N \end{cases} \quad (6)$$

where  $F_0$  and  $F_1$  are the state evolution functions introduced in (1), and  $N$  is the total number of joint CV signals. In this terminology, the superscripts point to a specific CV signal (1 for ECG, 2 for ABP, 3 for PPG, and so forth).

In order to establish correlation between the  $2N$  state variables in (5), it is necessary to force a relationship between the parameters of the model. This relationship can be found either with respect to the spatial/temporal locations of specific points in the signals, or even by considering the intrinsic consequential interdependences of the signals. In a hospital setting, patients are usually stationary and often sedated, which cause the heart rate to be a quasi-periodic signal with slowly varying fundamental frequencies, amplitudes, and morphologies. Since this periodicity is represented in the angular frequency of the signal, we propose a phase relationship between the corresponding state variables of the CV signals. Note that the observation signals  $\phi_k^j$  ( $j = 1, 2, \dots, N$ ) are synthetic saw-tooth shape signals that are found by detecting the  $R$ -peaks of the noisy CV measurements and linearly assigning a phase between  $-\pi$  and  $\pi$  to the samples between two successive  $R$ -peaks [21]. This signal is, in fact, a means of modeling the pseudoperiodic behavior of the cardiac dipole as it evolves during the depolarization and repolarization stages of the cardiac cycle.

Relating the phase signals has a physiological congruity with the nature of CV signals. In fact, the effect of the electrical impulse of the heart muscle is first seen on the ECG signal, and after specific delays, it is observed on other CV signals. Accordingly, we assume that the second to  $N$ th phase signals, i.e.,  $\phi_k^j$  ( $j = 2, \dots, N$ ), are shifted variants of the first phase signal ( $\phi^{\text{ECG}}$ ). Visual inspection of the characteristic waveforms in synchronous pairs of recorded CV signals reveals that the phase delays are equal to the angular distance between the  $R$  peaks of the signals. Hence, the phase state variables in (5) can be related to the first state variable as

$$\varphi_k^j = \varphi_k^1 - \Delta\theta_{R_k}^j, \quad j = 2, \dots, N, \quad (7)$$

where  $\Delta\theta_{R_k}^j = \theta_{R_k}^j - \theta_{R_k}^1$ . Since  $R_{\text{ECG}}$  is assumed to be at  $\theta_{R_k}^1 = \theta_{R_k}^{\text{ECG}} = 0$  (see [20] and [21] for detailed explanations about the phase signal), (7) reduces to

$$\varphi_k^j = \varphi_k^1 - \theta_{R_k}^j, \quad j = 2, \dots, N. \quad (8)$$

Based on the previous proposal, the timing and rates of the signal components are controlled by one phase variable and the second to  $N$ th phase variables become redundant. Similarly, it is possible to use only the first observation phase signal  $\phi_k^1$  since we need to track and estimate the CV measurements and not their phase values. On the other hand, the heart rate has an approximately equal effect on CV tachograms. Hence, it is

possible to assume equal angular frequencies for the CV signals. Therefore, the  $\omega_k^j$  terms are replaced by a single variable  $\omega_k$ . Accordingly, the simplified correlated nonlinear joint dynamics with reduced number of state variables is given by

$$\begin{cases} \varphi_{k+1}^1 = F_0(\varphi_k^1, \omega_k, k) \\ s_{k+1}^1 = F_1(s_k^1, \varphi_k^1, \alpha_i^1, b_i^1, \theta_i^1, \eta_k^1, \omega_k, k) \\ s_{k+1}^2 = F_1(s_k^2, \varphi_k^2, \alpha_i^2, b_i^2, \theta_i^2, \eta_k^2, \omega_k, k) \\ \vdots \\ s_{k+1}^N = F_1(s_k^N, \varphi_k^N, \alpha_i^N, b_i^N, \theta_i^N, \eta_k^N, \omega_k, k). \end{cases} \quad (9)$$

Similarly, the reduced linear observation relations are shown in matrix form as follows:

$$\begin{bmatrix} \phi_k^1 \\ z_k^1 \\ z_k^2 \\ \vdots \\ z_k^N \end{bmatrix} = \begin{bmatrix} 1 & 0 & 0 & \cdots & 0 \\ 0 & 1 & 0 & \cdots & 0 \\ 0 & 0 & 1 & \cdots & 0 \\ & & & \ddots & \\ 0 & 0 & 0 & 0 & 1 \end{bmatrix} \begin{bmatrix} \varphi_k^1 \\ s_k^1 \\ s_k^2 \\ \vdots \\ s_k^N \end{bmatrix} + \begin{bmatrix} u_{1_k}^1 \\ u_{2_k}^1 \\ u_{2_k}^2 \\ \vdots \\ u_{2_k}^N \end{bmatrix}. \quad (10)$$

Based on the equation sets (9) and (10), the vector components of the state-space formulation are defined as follows:

$$\begin{aligned} \underline{x}_k &= [\varphi_k^1 \quad s_k^1 \quad \cdots \quad s_k^N]' \\ \underline{y}_k &= [\phi_k^1 \quad z_k^1 \quad \cdots \quad z_k^N]' \\ \underline{w}_k &= [\alpha_{i_k}^1, b_{i_k}^1, \theta_{i_k}^1, \eta_k^1, \dots, \alpha_{i_k}^N, b_{i_k}^N, \theta_{i_k}^N, \eta_k^N, \omega_k]' \\ \underline{v}_k &= [u_{1_k}^1 \quad u_{2_k}^2 \quad \cdots \quad u_{2_k}^N]'. \end{aligned} \quad (11)$$

The joint dynamical model (9) includes a phase signal that controls the timings and produces the pseudoperiodicity of the heart cycle. Moreover,  $N$  different coupled GMM representations are provided for morphology assignment to the events of the CV signals. In fact, quasi-periodicity of the CV signals is reflected by the movement of the trajectories around the attracting limit cycle in phase plane, while the interbeat morphological variation is reproduced using its motion in terms of GMM parameters. These two basic components ( $\varphi$  and  $s$ ) are the essential variables of a dynamical state-space formulation that aims at integrating the temporal characteristics of each CV signal.

### III. BAYESIAN STATE ESTIMATION USING AN EXTENDED KF

The joint dynamical model (9) is a nonlinear function of the state and process noise vectors. Therefore, nonlinear extensions of the KF are required for estimating the state vector  $\underline{x}$ , using the process functions  $f$ , (9), and the observation functions  $g$ , (10). Our proposed framework is built upon an extended KF (EKF) structure for its simplicity and improved numerical stability over other Bayesian filters. However, other generalizations of the KF recursions to nonlinear state-space models have been developed such as the unscented KF [22] and particle filters [23], which could be also applied to this model. The EKF is based on a local linear approximation of the state-space model about an estimate of the state. The time and measurement propagation recursions

of EKF are summarized as follows [24]:

$$\begin{cases} \hat{x}_k^- = f(\hat{x}_{k-1}^+, \underline{w}, k)|_{\underline{w}=\hat{w}_k} \\ H_k^- = A_{k-1}H_{k-1}^+A_{k-1}' + B_{k-1}Q_{k-1}B_{k-1}' \\ \hat{x}_k^+ = \hat{x}_k^- + K_k r_k \\ K_k = H_k^- M_k' [M_k H_k^- M_k' + N_k R_k N_k']^{-1} \\ r_k = y_k - g(\hat{x}_k^-, v, k)|_{v=\hat{v}_k} \\ H_k^+ = H_k^- - K_k M_k H_k^- \end{cases} \quad (12)$$

where  $\hat{x}_k^- = E\{x_k | y_{k-1}, \dots, y_1\}$  is the *a priori* estimate of the state vector  $x_k$  at the  $k$ th stage using the observations  $y_1$  to  $y_{k-1}$ , and  $\hat{x}_k^+ = E\{x_k | y_k, \dots, y_1\}$  is the *a posteriori* estimate of this state vector after using the  $k$ th observation  $y_k$ .  $H_k^-$  and  $H_k^+$  are defined in the same manner to be the estimations of the covariance matrices, in the  $k$ th stage, before and after using the  $k$ th observation, respectively [25]. The linear approximate coefficients in (12) are defined as follows:

$$\begin{aligned} A_k &= \left. \frac{\partial f(\underline{x}, \hat{w}_k, k)}{\partial \underline{x}} \right|_{\underline{x}=\hat{x}_k} & B_k &= \left. \frac{\partial f(\hat{x}_k, \underline{w}, k)}{\partial \underline{w}} \right|_{\underline{w}=\hat{w}_k} \\ M_k &= \left. \frac{\partial g(\underline{x}, \hat{v}_k, k)}{\partial \underline{x}} \right|_{\underline{x}=\hat{x}_k} & N_k &= \left. \frac{\partial g(\hat{x}_k, \underline{v}, k)}{\partial \underline{v}} \right|_{\underline{v}=\hat{v}_k} \end{aligned} \quad (13)$$

in which  $A_k$  and  $B_k$  are the linearization coefficients with respect to the process equation (9), and  $M_k$  and  $N_k$  are the linearization coefficients with respect to the observation equation (10) [26]. Since the observation relationship is linear,  $M_k$  and  $N_k$  are  $(N+1) \times (N+1)$  and  $(N+1) \times (4N+1)$  identity matrices, respectively. However, in order to set up an EKF model based on the nonlinear model (9), it is necessary to have a linearized version of the state-space representation. Using (9) and (13), the following equations represent the linearized model with respect to the process components (i.e., the elements of  $B_k$ ):

$$\begin{aligned} \frac{\partial F_0}{\partial \alpha_i^j} &= \frac{\partial F_0}{\partial b_i^j} = \frac{\partial F_0}{\partial \theta_i^j} = \frac{\partial F_0}{\partial \eta_i^j} = 0 & j &= 1, \dots, N \\ \frac{\partial F_0}{\partial \omega} &= \delta & \frac{\partial F_1}{\partial \eta_i^j} &= 1 \\ \frac{\partial F_1}{\partial \omega} &= -\delta \text{GMM}(\alpha_i^j, b_i^j, \Delta\theta_i^j, k) \\ \frac{\partial F_1}{\partial \alpha_i^j} &= -\delta \omega_k \frac{\Delta\theta_i^j}{(b_i^j)^2} \exp\left(-\frac{1}{2} \left(\frac{\Delta\theta_i^j}{b_i^j}\right)^2\right) \\ \frac{\partial F_1}{\partial b_i^j} &= 2\delta \omega_k \frac{\alpha_i^j \Delta\theta_i^j}{(b_i^j)^3} \left(1 - \frac{1}{2} \left(\frac{\Delta\theta_i^j}{b_i^j}\right)^2\right) \exp\left(-\frac{1}{2} \left(\frac{\Delta\theta_i^j}{b_i^j}\right)^2\right) \\ \frac{\partial F_1}{\partial \theta_i^j} &= \delta \omega_k \frac{\alpha_i^j}{(b_i^j)^2} \left(1 - \left(\frac{\Delta\theta_i^j}{b_i^j}\right)^2\right) \exp\left(-\frac{1}{2} \left(\frac{\Delta\theta_i^j}{b_i^j}\right)^2\right). \end{aligned} \quad (14)$$

Similarly, the linearization of (9) with respect to the state variables yields

$$\begin{aligned} \frac{\partial F_0}{\partial s_k^j} &= 0 & \frac{\partial F_0}{\partial \phi_k^1} &= \frac{\partial F_1}{\partial s_k^j} = 1 & j &= 1, \dots, N \\ \frac{\partial F_1}{\partial \phi_k^1} &= -\delta \omega_k \text{GMM}\left(\alpha_i^j \left(1 - \left(\frac{\Delta\theta_i^j}{b_i^j}\right)^2\right), b_i^j, \Delta\theta_i^j, k\right). \end{aligned} \quad (15)$$

The EKF recursive algorithm requires an initial estimate of the state vector  $\hat{x}_0^-$  and the initial state covariance matrix  $H_0^-$ . In order to automate the parameter selection procedure for any given pairs of CV signals, the parameters should be estimated from the signals themselves. For this, the noisy observations may be transformed to a 3-D representation by plotting the noisy signal versus the periodic phases that are assigned to each sample in polar coordinates on the unit circle. In order to estimate the dynamical model parameters for the given observations, the mean and variance of the phase-wrapped signals are calculated for all phases between  $-\pi$  and  $+\pi$ . This gives the average of the phase-wrapped CV waveforms. To find the optimal parameters of (9) that can best fit the mean CV signals, a nonlinear least-squares approach is used to find the best MMSE estimate. To calculate the covariance values of  $Q_k$  and  $R_k$ , magnitude of the deviation of the parameters of the Gaussian functions around the estimated mean that best model the acceptable deviations of the signal around the mean signal is computed. The noise sources are assumed to be uncorrelated with each other to have simplified diagonal matrices. This parameter estimation procedure was previously detailed in [21] for a single ECG signal. The same methodology can be extended to other CV signals, where the optimization is based on the prior knowledge of the locations of the corresponding Gaussian kernels (8), which yields a constrained optimization.

#### IV. LIFE-THREATENING ARRHYTHMIA VERIFICATION

In this section, we demonstrate the utility of our proposed novel dynamical model for the verification of life-threatening arrhythmias in ICU patients, based on the standards of the Association for the Advancement of Medical Instrumentation (AAMI) [27]. The verification procedure is performed in two steps: anomaly detection and abnormality status determination. In the proposed framework, the morphological changes induced by the abnormalities can lead to large errors in the Gaussians functions' parameters, yielding unsatisfactory EKF estimates. Hence, by monitoring the state estimates' covariance matrices and the variations of the innovation signals, it is possible to detect such unexpected abnormalities. Accordingly, we define some signal fidelities by tracking the covariance matrix of  $r_k$  [see (12)] throughout the filtering procedure to detect morphological changes. Therefore, the EKF estimator is used as a signal quality index (SQI) for intelligent detection of abnormal beats. However, similar to the previously introduced SQIs in the literature [16], [28]–[30], the proposed  $N$ -dimensional signal fidelity does not distinguish between anomalies arising from physiologic disturbances such as an arrhythmia and

nonphysiologic phenomena such as noise. Hence, we benefit from the previously introduced polargram representation [31] for discrimination between artifacts and real rhythm changes, and hence, for abnormality status determination. Accordingly, for life-threatening arrhythmia verification, we adopt a two-stage procedure including the anomaly detection using the signal fidelity and abnormality determination using the polargram.

### A. Anomaly Detection

Various approaches toward determining the fidelity of the Bayesian filter estimations to the underlying dynamics of the corresponding state-space representation have been studied in the literature. A simple approach is to monitor the variance of the state estimations provided by the KF [32]. In practice, due to the Gaussian assumption on the noise sources and the initial state vector values, the state estimate entries of  $\hat{x}_k^+$  should lie within the envelope of the square roots of their corresponding diagonal entries in  $H_k^+$  for the majority of the time. Therefore, the variance of the state estimations provides a means of anomaly detection. Another approach to provide a means of monitoring the fidelity of the filter is to update the values of  $Q_k$  and  $R_k$  by monitoring the covariance matrix of the innovation signal throughout the filtering procedure and to compare it to the innovation covariance matrices estimated by the KF [33]. Specifically, with a diagonal (or diagonalized) noise covariance matrix of  $R_k$ , the signal fidelity for the  $j$ th CV signal observation in an averaging window of length  $L$  can be formed as follows:

$$\gamma_k^j = \frac{1}{L} \sum_{\ell=k-L+1}^k \frac{(r_\ell^j)^2}{E\{(r_\ell^j)^2\}}, \quad j = 1, 2, \dots, N, \quad (16)$$

where  $r_\ell^j$  is the  $j$ th entry of the zero-mean innovation vector defined in (12), corresponding to the  $\ell$ th sample of the  $j$ th CV signal measurement, with the KF estimated variance of

$$E\{(r_\ell^j)^2\} = (m_\ell^{j+1})' H_\ell^- m_\ell^{j+1} + \sigma_{(u_{j+1})_\ell}^2, \quad j = 1, 2, \dots, N, \quad (17)$$

where  $m_\ell^{j+1}$  is the  $(j+1)$ th row of the linearization matrix  $M$  defined in (13), and  $\sigma_{(u_{j+1})_\ell}^2 = E\{(u_{j+1})_\ell^2\}$  is the  $(j+1)$ th diagonal entry of  $R_k$ . In fact,  $\gamma^j$  is an average of the variances of the  $L$  recent innovations, normalized by their KF estimated variances of the  $j$ th CV signal that accounts for the joint information of coupled CV measurements. It is worth noting that as long as the morphology of the CV signal measurements remains normal,  $\gamma_k \approx 1$ . Values much greater than unity indicate that the innovation signal variance is being underestimated by the KF that confirms the presence of anomaly. Hence, the morphological changes may be simply identified and localized by monitoring the  $\gamma^j$  signals and using an adaptive threshold  $\text{thr}^j$ . The value of  $\text{thr}^j$  is defined to be at least  $\beta_1$  times the mean value of  $\gamma^j$  and to preserve  $\beta_2$  percent of the  $\gamma^j$  energy. In other words, with  $L_s$  be the length of the signal fidelity, the thresholds should satisfy the following conditions:

$$\begin{cases} \text{thr}^j \geq \beta_1 \bar{\gamma}^j \\ \forall k \gamma_k^j \leq \text{thr}^j : \quad \sum_k |\gamma_k^j|^2 = \beta_2 \sum_{k=1}^{L_s} |\gamma_k^j|^2. \end{cases} \quad (18)$$

TABLE I  
ALARM DEFINITIONS AND THRESHOLDS ACCORDING TO THE AAMI-EC-13  
CARDIAC MONITOR STANDARDS [27]

Alarm type	Detection criteria	Time delay for alarm
Asystole (AS)	No QRS for 4 sec	< 10 sec
Extreme bradycardia (BR)	HR < 40	< 10 sec
Extreme tachycardia (TA)	HR > 140	< 10 sec
Ventricular tachycardia (VT)	min 5 VT with HR > 100	N/A
Ventricular fibrillation (VF)	Fibrillatory waveform for min 4 sec	< 10 sec

### B. Abnormality Status Determination

Sayadi *et al.* proposed a polar representation, namely the *polargram*, which was used for premature ventricular contraction (PVC) detection [31]. The polargram shows the beat-to-beat variations during different cycles. In addition, by analyzing a specific portion of the polar plane, it is possible to investigate the interbeat morphological variations. Since our proposed framework is built upon a Bayesian filter, it is possible to form the polargram for all of the  $N$  CV signals by polar plotting the samples of the EKF estimations, as the amplitude, versus their corresponding phase values.

In order to investigate the status of abnormalities, we have focused on the determination of life-threatening arrhythmias, which produce a “red” critical alarm in commercial ICU monitoring systems. According to the current ANSI/AAMI EC13 Cardiac Monitor Standards [27], there are five categories of critical life-threatening arrhythmias, as illustrated in Table I.

At the onset of each anomaly (if detected by the signal fidelity), 25-s waveform segments were extracted, including 15 s prior to the anomaly onset and 10 s after the anomaly, from each of the  $N$  CV signals. Afterward, polargrams of the CV signals were formed and the anomaly was processed as follows.

1) *Asystole Processing*: To decide on the occurrence of an asystole (AS), the normal segment within the analysis window was used to compute the envelope of the polargram (i.e.,  $\bar{s}^j \pm 3\sigma_{s^j}$ ). In the case of AS, the polargram of the abnormal segment is expected to show no peaks in the phase plane. Hence, if the polar representation of the abnormal segment appeared below the envelope (in the region defined by  $[0 \quad \bar{s}^j - 3\sigma_{s^j}]$ ), and if the largest pulse-to-pulse interval within the analysis window was greater than 4 s, the anomaly was accepted as AS.

2) *Extreme Bradycardia Processing*: To verify the occurrence of an extreme bradycardia (BR), the longest pulse-to-pulse time intervals extracted from the  $N$  CV signals in the analysis window were used to estimate the mean heart rate. If the mean time required to complete consecutive high-quality (determined via the signal fidelity) cycles of the polargrams was above an adjustable threshold (here 1.5 s), which corresponds to mean HR below 40 BPM, the anomaly is accepted as BR.

3) *Extreme Tachycardia Processing*: To determine the occurrence of an extreme tachycardia (TA), the shortest pulse-to-pulse time intervals extracted from the  $N$  CV signals in the analysis window were used to estimate the mean heart rate. If

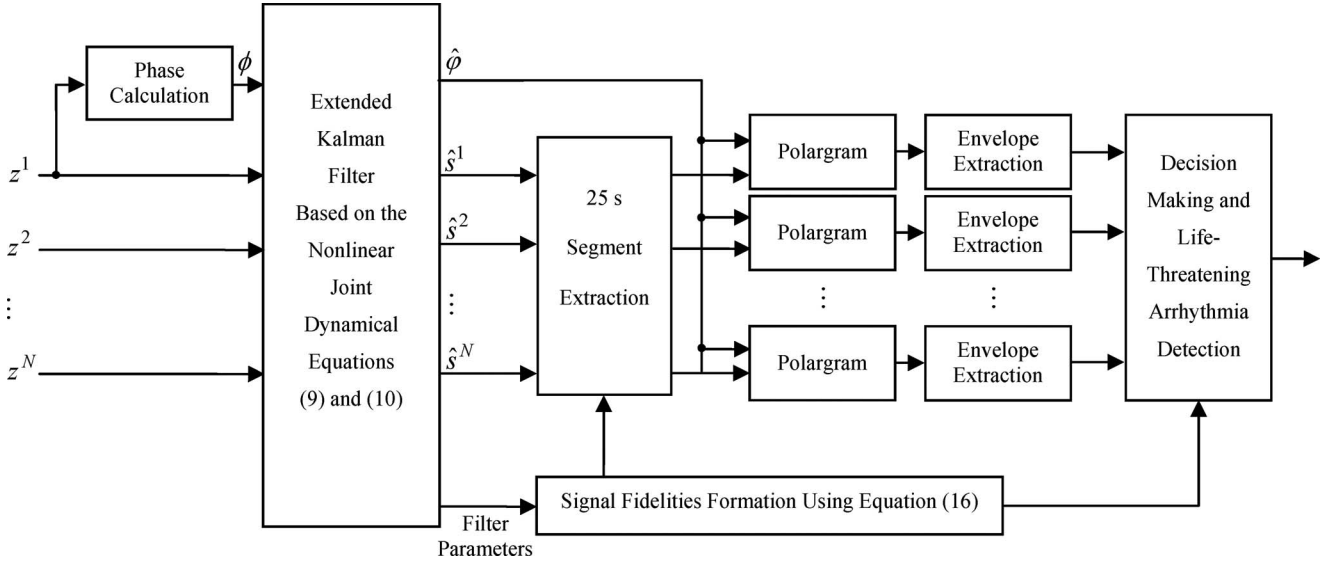


Fig. 1. General block diagram of the proposed algorithm for life-threatening arrhythmia verification.

the mean time required to complete consecutive high-quality cycles of the polargrams was below an adjustable threshold (here 0.42 s), which corresponds to mean HR above 140 BPM, the anomaly is accepted as TA.

4) *Ventricular Tachycardia Processing*: The anomaly was decided as ventricular tachycardia (VT) if the following conditions held: 1) the mean time required to complete consecutive high-quality cycles of the polargrams was below an adjustable threshold (here 0.6 s); 2) the QRS widening was observed in the phase plane representation in all CV polargrams; and 3) the signal fidelities denote abnormal behavior for at least 3 s (corresponding to minimum 5 VT with HR > 100).

5) *Ventricular Fibrillation Processing*: The anomaly was decided as ventricular fibrillation (VF) if both conditions are satisfied: 1) the mean time required to complete consecutive cycles of the polargrams was below an adjustable threshold (here 0.6 s); 2) the abnormal behavior (as judged by the signal fidelity) lies outside the polar envelope for at least 3 s.

The overall life-threatening arrhythmia verification algorithm is shown in Fig. 1, in which the phase calculation block is simply an  $R$ -peak location detector, followed by linear assigning of a phase value between  $-\pi$  and  $\pi$  to the intermediate samples [21]. The decision-making block uses the polargrams and the signal fidelities to detect arrhythmia occurrence. In fact, we use (18) to compute the values of the thresholds using the fidelity signals. Afterward, the thresholding is performed to locate  $\gamma^j$  peaks. Finally, the polargrams together with the signal fidelities are processed based on the proposal in Section IV-B to verify the status of abnormal behaviors.

## V. SIMULATION RESULTS

In this section, the detection properties of our proposed joint dynamical model are demonstrated and the EKF estimator is used for robust verification of critical arrhythmias. We provide examples that illustrate the ability to solve relevant prob-

lems in cardiac abnormality verification including the detection, status determination, and false alarm suppression. The proposed algorithm was implemented in MATLAB and the PhysioNet's MIMIC I database [34], [35] and MIMIC II waveform database [36], [37] were used for performance evaluation. Qualitative and quantitative results are presented next.

Fig. 2 shows a typical set of ICU records and their EKF estimates including the ECG, ABP, PPG, CVP, PAP, and ART. Also, two typical polargrams (the ECG polargram and the PPG polargram) are also depicted. Visual inspection reveals that the signal fidelities can easily locate the anomalies. Also, the inter-beat morphological changes are replicated in the polargrams, which facilitate the arrhythmia detection procedure.

Receiver operating characteristics had been performed to select possibly optimal values of thresholding variables  $\beta_1$  [multiplier of the mean value in (18)] and  $\beta_2$  [multiplier of the energy value in (18)]. The search was restricted to parameter values that resulted in the highest abnormality true positive (TP) detection rate [namely, sensitivity (Sn)] and lowest false positive (FP) detection rate [namely, one minus specificity (Sp)]. Fig. 3 illustrates the 2-D (two-parameter) optimization approach using 50 patient records of variable length containing simultaneously recorded CV signals from the MIMIC I database. It can be seen that as the parameter  $\beta_1$  was increased from 0 to 5, the FP detection rate increased steadily to 0. Moreover, for  $0.9 < \beta_2 < 0.98$ , the TP detection rate continues to rise, with a rapidly decreasing FP detection rate. In this case, the best values that gave the maximum TP and the minimum FP detection rates were chosen as  $\beta_1 = 2.8$  and  $\beta_2 = 0.92$ , respectively.

For data analysis, a subset of records was selected from the first 498 records in the MIMIC II database that excludes patients who had active intra-aortic balloon pumps and fulfilled the following two criteria: 1) a critical ECG arrhythmia alarm ("red alarm") was issued during the ICU stay; and 2) at least one channel of ECG, an ABP waveform, a PPG signal, and a CVP or PAP waveform were present at the time of the arrhythmia alarm.

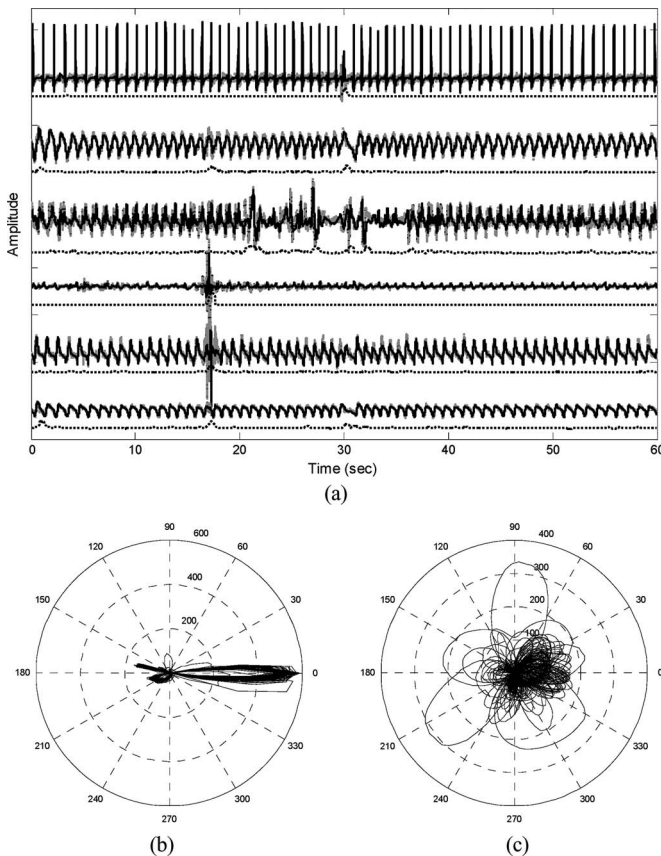


Fig. 2. Bayesian estimation and abnormality detection using the proposed joint dynamical framework. (a) Typical ICU data and their EKF estimates; from top to bottom: ECG, ABP, PPG, CVP, PAP, and ART. Signal fidelity corresponding to each signal is shown under the same signal by a dotted time series. (b) ECG polargram. (c) PPG polargram.

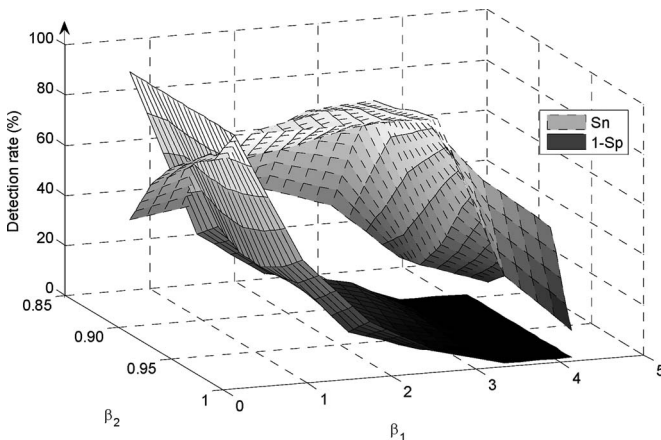


Fig. 3. TP (dotted) and FP (dashed) detection rates for Bayesian arrhythmia detection as a function of the two variables  $\beta_1$  and  $\beta_2$ .

The final test set comprised 1500 life-threatening arrhythmias. The distribution of the critical ECG abnormalities and the detection results are detailed in Table II, in which the number of registers per rhythm type is shown by  $N_{\text{abn}}$ . To express how successfully the Bayesian classifier recognizes abnormal beats of a certain class without missing them, sensitivity measure was used. Likewise, to measure how exclusively it classifies beats of

TABLE II  
LIFE-THREATENING ARRHYTHMIA DETECTION RESULTS USING THE PROPOSED BAYESIAN ALGORITHM

Type	$N_{\text{abn}}$	Dataset					
		Type A		Type B		Type C	
		Sn (%)	+P (%)	Sn (%)	+P (%)	Sn (%)	+P (%)
AS	50	100.00	100.00	100.00	100.00	100.00	100.00
BR	300	100.00	97.09	100.00	99.34	100.00	100.00
TA	500	100.00	97.85	100.00	99.21	100.00	99.40
VT	600	93.50	97.73	97.83	98.50	99.17	98.67
VF	50	96.00	100.00	98.00	100.00	98.00	100.00
Total	1500	97.27	97.79	99.07	99.00	99.60	99.27

a certain type, positive predictivity (+P) was used. Moreover, to investigate the effect of joint interdependent information provided by the CV signals, the test dataset included different sets of synchronous records; records including ECG and ABP (type A), records of ECG, ABP, and PPG (type B), and records including ECG, ABP, PPG and at least one other CV signal such as PAP or CVP (type C). As can be observed from the table, the TP detection rate (Sn) ranges over 93.50% and 100.00%, while the FP detection rate ranges over 97.09% and 100%, which are well within the acceptable range [38]. The last four columns of the table show the capability of the interdependent information provided by the extra CV signals to improve the arrhythmia verification results. In particular, adding the PPG signal to the ECG–ABP pair (type B) has caused a significant improvement in the sensitivity of the VT detection. However, the addition of other CV signals such as PAP or CVP has improved the positive predictivity of the proposed method. In a global quantification, the proposed method has the maximum sensitivity equal to 99.60% and the maximum positive predictivity equal to 99.27% for the total arrhythmic types.

To appreciate the merits of the proposed method over conventional life-threatening arrhythmia detection algorithms, we have compared our results to those of some benchmark techniques in the literature. Recently, Aramendi *et al.* [39] reviewed the previously introduced ECG morphological parameters [12], [13] and spectral variables [14], [15] for life-threatening arrhythmia detection. A comparative study of the results is reported in Table III, which shows that our proposed method provides a higher sensitivity, while preserving the specificity in the acceptable range. Moreover, taking the number of analyzed abnormalities into consideration, it can be definitely said that the results of our algorithm are comparable to and usually superior to the other methods, which show the ability of the proposed framework to distinguish the critical arrhythmias more accurately.

Another interesting feature of the proposed verification method is its ability to determine the status of the alarms issued by the bedside monitors in ICUs. This way, the method would be capable of suppressing falsely issued alarms, which disrupt patients' rest, drain hospital resources, and desensitize the hospital staff to potential emergency situations [40]. It has been estimated that 43% of life-threatening ECG alarms issued by bedside monitors are false, with some categories of alarm being as high as 90% [17]. These false arrhythmia alarms (FA)

TABLE III  
PERFORMANCE COMPARISON OF BENCHMARK METHODS FOR  
LIFE-THREATENING ARRHYTHMIA DETECTION [39] TO THE RESULTS  
OF THE PROPOSED BAYESIAN TECHNIQUE

Methods	Parameters	Type			
		AS	BR	VT	VF
<i>Threshold</i>	$N_{abn}$	10	22	81	200
<i>crossing interval</i>	$S_n$	N/A	N/A	43.20	88.50
[12]	$S_p$	100.00	90.90	N/A	N/A
<i>Complexity</i>	$N_{abn}$	10	22	81	200
<i>Measure</i>	$S_n$	N/A	N/A	29.60	92.50
[13]	$S_p$	100.00	95.50	N/A	N/A
<i>Spectral energy</i>	$N_{abn}$	10	22	81	200
<i>distribution</i>	$S_n$	N/A	N/A	100.00	89.00
[14]	$S_p$	90.00	95.50	N/A	N/A
<i>VF-filter</i>	$N_{abn}$	10	22	81	200
<i>leakage</i>	$S_n$	N/A	N/A	96.30	91.00
[15]	$S_p$	70.00	100.00	N/A	N/A
<i>Proposed</i>	$N_{abn}$	50	300	600	50
<i>Bayesian</i>	$S_n$	100.00	100.00	96.83	97.33
<i>method</i>	$S_p$	100.00	98.81	98.30	100.00

are often due to single channel ECG noise and artifacts, and therefore, it is likely that the FA rates may be reduced if information from other CV signals is used to form a more robust hypothesis of the alarm's etiology. Aboukhalil *et al.* created an algorithmic framework that consulted the ABP waveform to corroborate critical ECG arrhythmia alarms [17]. This framework was then extended to incorporate the information provided by the PPG signal [16]. However except for AS, the PPG-based false alarm suppression system did not perform as well as the ABP-based suppression technique.

The proposed Bayesian verifier can effectively consult the interdependent information of the CV signals for robust determination of alarms' status. Hence, after the onset of any ECG critical alarm, the same verification procedure as shown in Fig. 1 is performed to FA suppression.

Unlike other previous investigations into reducing false alarms in ICU data, which are relatively few and were performed on small datasets, the recent studies in [16] and [17] have used a subset of the MIMIC II database for performance evaluation. The subset was chosen among 498 records whose alarms were annotated as either "True" or "False" by expert human review [17]. Similarly, we have used the same database (MIMIC II) to study the suppression method; however, due to the multi-signal nature of our proposed framework, we have excluded ECG signals which were not accompanied by ABP, PPG, and CVP/PAP waveforms. Hence, the distribution of alarms may be different compared to [17] (which is based on ECG-ABP pairs) and [16] (which is based on ECG-ABP-PPG waveforms). Table IV details the results of the proposed Bayesian algorithm and a comparison to the best previously published results [17]. It can be observed that the FA suppression rates for the proposed method ranges between 62.3% and 98.0%, while preserving the true alarms (TA) unchanged, except for the VT. The last two columns of Table IV provide the FA rates before and after suppression. It can be seen that the asystole FA rates were reduced from 86.5% to 1.7%. The FA rates of BR and TA rates were

reduced from 25.0% and 16.7% to 6.4% and 4.7%, respectively. The false VT alarm suppression rates were reduced from 44.4% to 14.8%, at the cost of suppressing 3.8% of the true VT. The false VF alarm suppression rate was the lowest of all alarm categories tested, with a reduction in the FA rate from 66.7% to 25.1. No true alarms were suppressed for any other critical alarm group in this study, except the VT. The overall FA rate was reduced from 42.3% to 9.9%. Compared to [17], it can be said that the proposed Bayesian verification procedure is more efficient, since it used an adaptive fidelity and was based on the interdependences of  $N$  CV signals. It should be noted that despite the difference in the number of alarms (between our subset and the one used in [17]), the ratios of each arrhythmia type to the total number of arrhythmias are comparable for both methods. In particular, the relative distributions of all true and false alarms for our dataset are 57.7% and 42.3%, respectively, wherein [17], these ratios are 57.3% and 42.7%, respectively, which shows that relative comparison of the results could be fair.

As an advantage, the proposed EKF structure provides a means of measuring the fidelity of the filter estimates, which is a sort of intrinsic signal quality measure in the Bayesian architecture. In contrast, the use of the ABP waveform [17] or even the PPG record [16] required the corresponding signal quality measures, which in turn was depended on the incorporation of information extracted from the waveform into the ECG false alarm suppression framework and required assessment of the beat onset to avoid drawing misleading information from an artifactual waveform. Despite these advantages, the method suffers from two sources of detection errors. Detection failures may occur as the result of the thresholding or the missed  $R$ -peaks. The former is an unavoidable source of error in all threshold-based schemes that results in errors in verifying the fidelity onset, while the latter is as the result of morphology variations. In fact, when an  $R$ -peak is misdetected, the phase error of the model can lead to large errors in the Gaussian functions' locations. For such occasional errors, even temporal adaptation of the filter parameters is not helpful, as the filter does not have sufficient time to adapt itself. Hence, an unexpected fidelity rise, as well as a FP detection will occur. Fig. 4(a) shows an example of FN detections, where the presence of a dominant ectopic has influenced the threshold value, which results in missing the VT beats. Fig. 4(b) demonstrates the effect of missed  $R$ -peaks (in both ECG and ABP), which gives rise in the fidelity values and, consequently, results in FP detections.

## VI. DISCUSSION AND CONCLUSION

A novel nonlinear joint dynamical set of state-space equations was proposed for modeling the interdependences of coupled CV signals that could be used with the generalizations of the KF for nonlinear state-space models, such as the EKF. The model is based on GMM representation of motion that incorporates the couplings of the frequency and phase information into a joint dynamical model, and linear observation relations.

Since the developed model consists of a set of state-space process equations and a set of observation relations, a Bayesian framework was proposed for the estimation and tracking of real CV signals based on this joint state-space model. From a

TABLE IV  
FALSE AND TRUE ALARM SUPPRESSION RESULTS OF THE PROPOSED BAYESIAN ALGORITHM WITH RESULTANT AVERAGE FALSE ALARM (FA) AND TRUE ALARM (TA) RATES. THE BEST PREVIOUSLY REPORTED RESULTS ([17]) ARE SHOWN IN PARENTHESIS

Type	Distribution of Alarms			Relative Distribution of Alarms (%)			Suppression rates (%)		FA rates (%)	
	True	False	Total	True	False	Total	TA	FA	Before	After
AS	50 (54)	320 (525)	370 (579)	3.3 (1.7)	29.1 (22.8)	14.2 (10.7)	0.0 (0.0)	98.0 (93.5)	86.5 (90.7)	1.7 (5.5)
BR	300 (507)	100 (210)	400 (717)	20.0 (16.4)	9.1 (9.1)	15.4 (13.3)	0.0 (0.0)	74.4 (81.0)	25.0 (29.3)	6.4 (5.5)
TA	500 (1444)	100 (433)	600 (1877)	33.3 (46.8)	9.1 (18.8)	23.1 (34.8)	0.0 (0.0)	72.1 (63.7)	16.7 (23.1)	4.7 (8.4)
VT	600 (1015)	480 (885)	1080 (1900)	40.0 (32.9)	43.6 (38.4)	41.5 (35.3)	3.8 (9.4)	66.7 (33.0)	44.4 (46.6)	14.8 (30.8)
VF	50 (64)	100 (249)	150 (313)	3.3 (2.1)	9.1 (10.4)	5.8 (5.6)	0.0 (0.0)	62.3 (58.2)	66.7 (79.6)	25.1 (33.1)
All	1500 (3084)	1100 (2302)	2600 (5386)	57.7 (57.3)	42.3 (42.7)	---	1.5 (2.4)	76.6 (59.7)	42.3 (42.7)	9.9 (17.2)

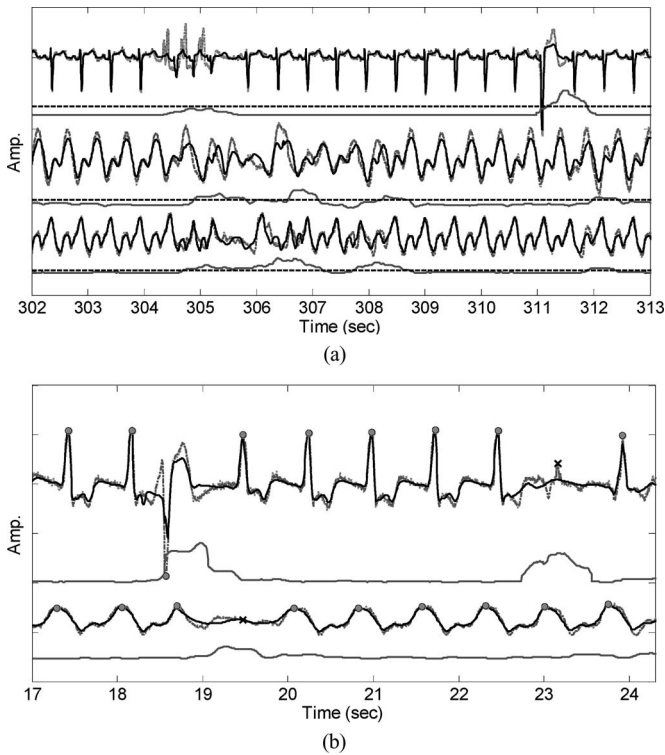


Fig. 4. Possible cases of algorithm failure for typical ICU data. (a) Thresholding error, from top to bottom: ECG, PPG, and ABP; the dotted line shows the threshold. (b) Misdetected  $R$ -peak, from top to bottom: ECG,  $\gamma^{ECG}$ , ABP and  $\gamma^{ABP}$ ; the circles show the detected  $R$ -peaks, while the cross shows the missed  $R$ -peak.

filtering point of view, KFs can be considered as adaptive filters that continuously move the location of the poles and zeros of their transfer functions, according to the signal or noise content of the input observations and the prior model of the signal dynamics. The filter structure is based upon a unique dynamical model, which is adapted to the observations according to the propagation equations. Moreover, this feature allows the filter to adapt with different spectral shapes and temporal nonstationarities, since the variance of the observation noise represents the degree of reliability of the observation as well as the degree of adaptively tracking the input noisy measurement. Based on this concept, we proposed the use of the innovation sequence to monitor the fidelity of the filter and to form the polar representation of the signals for life-threatening arrhythmia verification.

The proposed verification technique is, in fact, a novel generalization to the previously published Bayesian method for PVC detection [30], which provides a novel joint extension to the dynamical model and modifications in the detection procedure.

Performance evaluation results showed that the developed method provides reliable and accurate critical abnormality detection, with an average sensitivity of 99.60% and an average positive predictivity equal to 99.27%, which are well within the acceptable range, and is superior to the previously reported results. Moreover, in comparison to other published methods for life-threatening abnormality detection, our proposed approach provides a superior performance, while eliminating the need to employ threshold-based decision rules, feature extraction, training, and selection of the classifiers' structure.

Another point of interest is the capability of the algorithm to suppress the falsely issued alarms by the ICU bedside monitors. The false alarm suppression algorithm presented in this paper applies as a multistate extension of the system proposed by Aboukhalil *et al.* [17], which consults the interdependence of the coupled CV signals using a Kalman-based structure. In the present study, for patients with invasive CV monitoring, false critical ECG arrhythmia alarm rates in the ICU were found to be, on average, 42.3% with individual rates varying between 16.7% and 86.5%.

The proposed KF adaptive framework is influenced by the initial values for the state vector and the covariance matrices of the process and the measurement noise. The dependence of the estimated trajectories on these initial estimations is the major drawback of the proposed method. Hence, an automated procedure for reliable initialization was proposed. In addition, the threshold-based detection procedure as well as the  $R$ -peak misdetected may result in verification errors.

The recursive structure of the KF makes the algorithm computationally tractable, and hence, suitable for real-time applications. For the currently developed MATLAB code on a Corei7 CPU at 2.67 GHz, the computation time is close to real time. However, optimization of this code or conversion into low-level languages would result in a significant increase in performance speed. This would allow the algorithm to run on synchronous data in real time on most embedded ICU systems.

In summary, the main contributions of this work are as follows: 1) the introduction of a novel joint dynamical state-space formulation for modeling an  $N$ -dimensional coupled CV

measurements; 2) the derivation of a linearized model and the establishment of linear observation relations; 3) the proposal of a Kalman-based filtering scheme that could provide robust estimations of the input noisy measurements as well as the fidelity tracking; and 4) the abnormality verification (including the detection and status determination) based on the EKF parameters and the polar representation of the signals, which was further applied to ICU FA reduction. Future works include incorporating non-Gaussian dynamics into the model to have a physiological correspondence for the asymmetric waveforms. In addition, it is possible to use the proposed Bayesian framework for reliable denoising of CV signals. Moreover, it is possible to use the joint dynamical paradigm and the concept of Markov models to incorporate the transitions from normal to arrhythmia for monomorphic or polymorphic arrhythmia detection.

## REFERENCES

- [1] D. Dubin, *Rapid Interpretation of EKG's*. Tampa, FL: Cover, 2000.
- [2] M. J. Kern, M. J. Lim, and J. A. Goldstein (Eds.), *Hemodynamic Rounds: Interpretation of Cardiac Pathophysiology from Pressure Waveform Analysis*. Hoboken, NJ: Blackwell, 2009.
- [3] M. D. Cheitlin, M. Sokolow, and M. B. McIlroy, *Clinical Cardiology*: Appleton & Lange, Norwalk, Conn., 1993.
- [4] M. A. Cohen and J. A. Taylor, "Short-term cardiovascular oscillations in man: Measuring and modeling the physiologies," *J. Physiol.*, vol. 542, pp. 669–683, 2002.
- [5] H. P. Koepchen, "History of studies and concepts of blood pressure waves," in *Mechanisms of Blood Pressure Waves*, K. Miyakawa, C. Polosa, and H. P. Koepchen, Eds. Berlin, Germany: Springer-Verlag, 1984, pp. 3–23.
- [6] G. Baselli, E. Caiani, A. Porta, N. Montano, M. G. Signorini, and S. Cerutti, "Biomedical signal processing and modeling in cardiovascular systems," *Crit. Rev. Biomed. Eng.*, vol. 30, pp. 55–84, 2002.
- [7] R. Virmani, *Cardiovascular Pathology*. W. B. Saunders Co., Philadelphia, PA, 2001.
- [8] La. Rovere, "Methods to assess baroreflex sensitivity as a measure of the activity of the autonomic nervous system," in *Advances in Noninvasive Electrocardiograph Monitoring Techniques*, M. H.-H. Osterhues et al., Ed. Norwell, MA: Kluwer Academic Publishers, 2000.
- [9] M. L. Appel, R. D. Berger, J. P. Saul, J. M. Smith, and R. J. Cohen, "Beat to beat variability in cardiovascular variables: Noise or music," *J. Am. Coll. Cardiol.*, vol. 14, no. 5, pp. 1139–1148, 1989.
- [10] R. I. Kitney, T. Fulton, A. H. McDonald, and D. A. Linkens, "Transient interactions between blood pressure, respiration and heart rate in man," *J. Biomed. Eng.*, vol. 7, no. 3, pp. 217–224, 1985.
- [11] J. McNames and M. Aboy, "Statistical modeling of cardiovascular signals and parameter estimation based on the extended Kalman filter," *IEEE Trans. Biomed. Eng.*, vol. 55, no. 1, pp. 119–129, Jan. 2008.
- [12] N. Thakor, Y. S. Zhu, and K. Y. Pan, "Ventricular tachycardia and fibrillation detection by a sequential hypothesis testing algorithm," *IEEE Trans. Biomed. Eng.*, vol. 37, no. 9, pp. 837–843, Sep. 1990.
- [13] X. S. Zhang, Y. S. Zhu, N. Thakor, and Z. Z. Wang, "Detecting ventricular tachycardia and fibrillation by complexity measure," *IEEE Trans. Biomed. Eng.*, vol. 46, no. 5, pp. 548–555, May 1999.
- [14] S. Barro, R. Ruiz, D. Cabello, and J. Mira, "Algorithmic sequential decision-making in the frequency domain for life threatening ventricular arrhythmias and imitative artefacts: A diagnostic system," *J. Biomed. Eng.*, vol. 11, pp. 320–328, 1989.
- [15] S. Kuo and R. Dillman, "Computer detection of ventricular fibrillation," in *Computers in Cardiology*. Los Alamitos, CA: IEEE Comput. Soc. Press, 1978, pp. 347–349.
- [16] V. Deshmane, "False arrhythmia alarm suppression using ECG, ABP, and photoplethysmogram," M.Sc. thesis, Dept. Electr. Eng. Comput. Sci., MIT Univ., Cambridge, MA, 2009.
- [17] Aboukhalil, L. Nielsen, M. Saeed, R. G. Mark, and G. D. Clifford, "Reducing false alarm rates for critical arrhythmias using the arterial blood pressure waveform," *J. Biomed. Inform.*, vol. 41, pp. 442–451, 2008.
- [18] P. E. McSharry, G. D. Clifford, L. Tarassenko, and L. A. Smith, "A dynamic model for generating synthetic electrocardiogram signals," *IEEE Trans. Biomed. Eng.*, vol. 50, no. 3, pp. 289–294, Mar. 2003.
- [19] R. Sameni, M. B. Shamsollahi, and C. Jutten, "Filtering electrocardiogram signals using the extended Kalman filter," in *Proc. 27nd IEEE Eng. Med. Biol. (EMBS) Conf.*, Shanghai, China, Sep. 1–4, 2005, pp. 5639–5642.
- [20] R. Sameni, M. B. Shamsollahi, C. Jutten, and M. Babaie-Zadeh, "Filtering noisy ECG signals using the extended Kalman filter based on a modified dynamic ECG model," in *Proc. 32nd Annu. Int. Conf. Comput. Cardiol.*, Lyon, France, Sep. 25–28, 2005, pp. 1017–1020.
- [21] R. Sameni, M. B. Shamsollahi, C. Jutten, and G. D. Clifford, "A nonlinear Bayesian filtering framework for ECG denoising," *IEEE Trans. Biomed. Eng.*, vol. 54, no. 12, pp. 2172–2185, Dec. 2007.
- [22] E. A. Wan and R. Van Der Merwe, "The unscented Kalman filter," in *Kalman Filtering and Neural Networks*, S. Haykin, Ed. New York: Wiley, 2001.
- [23] P. M. Djuric, J. H. Kotecha, J. Zhang, Y. Huang, T. Ghirmai, M. F. Bugallo, and J. Míguez, "Particle filtering," *IEEE Signal Process. Mag.*, vol. 20, no. 5, pp. 19–38, Sep. 2003.
- [24] S. M. Kay, *Fundamentals of Statistical Signal Processing: Estimation Theory*. Englewood Cliffs, NJ: Prentice-Hall, 1993.
- [25] D. Simon, (ed.), *Optimal State Estimation*. New York: Wiley, 2006.
- [26] S. Haykin, (ed.), *Kalman Filtering and Neural Networks*. New York: Wiley, 2001.
- [27] *Cardiac Monitors, Heart Rate Meters, and Alarms*, American National Standard ANSI/AAMI EC13:2002. Association for the Advancement of Medical Instrumentation, Arlington, VA, 2002.
- [28] W. Zong, G. B. Moody, and R. G. Mark, "Reduction of false arterial blood pressure alarms using signal quality assessment and electrocardiogram-arterial blood pressure relationships," *Med. Biol. Eng. Comput.*, vol. 42, pp. 698–706, Sep. 2004.
- [29] J. X. Sun, A. T. Reisner, and R. G. Mark, "A signal abnormality index for arterial blood pressure waveforms," in *Proc. Comput. Cardiol.*, 2006, pp. 13–16.
- [30] J. X. Sun, "Cardiac output estimation using arterial blood pressure waveforms," M.Sc. thesis, Dept. Electr. Eng. Comput. Sci., MIT Univ., Cambridge, MA, 2006.
- [31] O. Sayadi, M. B. Shamsollahi, and G. D. Clifford, "Robust detection of premature ventricular contractions using a wave-based Bayesian framework," *IEEE Trans. Biomed. Eng.*, vol. 57, no. 2, pp. 353–362, Feb. 2010.
- [32] A. Gelb, (ed.), *Applied Optimal Estimation*. Cambridge, MA: MIT Press, 1974.
- [33] M. S. Grewal, L. R. Weill, and A. P. Andrews, (eds.), *Global Positioning Systems, Inertial Navigation, and Integration*. New York: Wiley, 2001.
- [34] G. B. Moody and R. G. Mark, "A database to support development and evaluation of intelligent intensive care monitoring," in *Proc. Comput. Cardiol.*, 1996, pp. 657–660.
- [35] The MIMIC Database. (2010, Jun. 30). [Online]. Available: <http://physionet.caregroup.harvard.edu/physiobank/database/mimicdb/>
- [36] M. Saeed, C. Lieu, G. Raber, and R. G. Mark, "MIMIC II: A massive temporal ICU patient database to support research in intelligent patient monitoring," in *Proc. Comput. Cardiol.*, 2002, vol. 29, pp. 641–644.
- [37] The MIMIC II Waveform Database. (2010, Jun. 30). [Online]. Available: <http://www.physionet.org/pn5/mimic2db/>
- [38] R. E. Kerber, L. B. Becker, J. D. Bourland, R. O. Cummins, A. P. Hallstrom, M. B. Michos, G. Nichol, J. P. Ornato, W. H. Thies, R. D. White, and B. D. Zuckerman, "Automatic external defibrillators for public access defibrillation: Recommendations for specifying and reporting arrhythmia analysis algorithm performance, incorporating new waveforms, and enhancing safety. A statement for health professionals from the American Heart Association Task Force on Automatic External Defibrillation, Subcommittee on AED Safety and Efficacy," *Circulation*, vol. 95, pp. 1677–1682, 1997.
- [39] E. Aramendi, U. Irusta, E. Pastor, A. Bodegas, and F. Benito, "ECG spectral and morphological parameters reviewed and updated to detect adult and paediatric life-threatening arrhythmia," *Physiol. Meas.*, vol. 31, pp. 749–761, 2010.
- [40] N. Thakor, Y. S. Zhu, and K. Y. Pan, "Ventricular tachycardia and fibrillation detection by a sequential hypothesis testing algorithm," *IEEE Trans. Biomed. Eng.*, vol. 37, pp. 837–843, 1990.